We sincerely thank the referee for the positive assessment of the scientific value and potential importance of our observations and for the constructive suggestions. We have carefully considered all the comments and have substantially revised the literature review, NPF-event classification, interpretation of the possible NPF mechanisms, analysis of local urban emissions, and figure presentation. Our point-by-point responses are provided below.

Comment 1:

Introduction:

The introduction is overall well structured; However, it might be that the literature review is somehow narrow. I do understand that the focus of the paper is the Tibetan Plateau however there are several other studies with a focus on high altitude measurements and location very close to the one done in this study. This introduction focuses strongly on recent Tibetan Plateau background studies while giving limited attention to the broader high-altitude and free-tropospheric NPF literature. I can imagine that a comparison done with measurements presented in Himalaya such as Bianchi et al. (2021, Nature Geoscience) but also many other studies could be good for this work. Also, this comparison can been done when discussing the possible precursors. In this way the authors can also benefit by distinguish their urban Lhasa case from other mountain NPF types.

Response 1：

Thank you for this helpful suggestion. We agree that the original Introduction focused primarily on recent studies conducted at background sites on the Tibetan Plateau and provided insufficient discussion of the broader high-altitude and free-tropospheric NPF literature.

We have therefore expanded the Introduction to include the Himalayan studies of Venzac et al. (2008) and Bianchi et al. (2021), as well as the free-tropospheric NPF and CCN-related observations conducted at the high-altitude Chacaltaya station by Rose et al. (2017). The added discussion highlights the roles of mountain-valley circulation, vertical transport, and organic precursor chemistry in NPF at remote high-altitude sites.

We have also further clarified the distinction between these remote mountain environments and the urban Lhasa site. Previous observations at remote Himalayan sites showed that up-valley transport can supply gaseous precursors, including biogenic organic compounds, thereby promoting particle formation and subsequent transport into the free troposphere. In contrast, the TU site is located in a high-altitude urban environment and is additionally influenced by traffic, combustion, construction activities, and anthropogenic gaseous precursors. This comparison more clearly demonstrates the novelty of the present study and provides a broader context for the subsequent discussion of potential NPF precursors.

Comment 2:

Classification event:

It is well known that the actual classification method is subjective and probably quite qualitative. However, I have the feeling that in this case can be improved. Also, because many central results depend on the classification, like NPF frequency, J/GR

statistics, and CCN formation. For example, in figure 2, I would even think that type II and even undefined can be considered as a class I event. Mostly, it seems that, the separation between Class II and Undefined events is not really clear. Something useful could be a day-by-day classification table, including event start/end times, growth-rate time windows, and so on. An additional approach could be to use a ranking method that classified that days in function of particles that have been produced.

Response 2：

We thank the referee for this important and constructive suggestion. We agree that the distinction between the original Class I and Class II events was not sufficiently robust and that the subjectivity of this separation could affect the reported NPF frequency, formation and growth rates, and estimated CCN concentrations.

Following the referee ' s suggestion, we re-examined the PNSD evolution for every observation day and removed the distinction between Class I and Class II. The two original categories were combined into a single "NPF day" category. The revised classification now consists of NPF, Undefined, and Non-Event days. Correspondingly, all major figures and statistical analyses involving event classification, including the NPF frequency, J/GR statistics, sink analysis, and estimated CCN concentrations, were recalculated using the revised three-category classification.

NPF days were identified primarily by the appearance of a distinct new particle mode at small diameters followed by identifiable growth toward larger sizes. Continuous growth throughout the entire day was not required, because temporary interruptions may result from changes in air masses, boundary-layer development, variations in precursor availability, or missing measurements. For days with weak, discontinuous, or ambiguous modal evolution, visual inspection of the PNSD was further supported by the mean particle number concentrations in the 3–25 and 25–100 nm size ranges and candidate particle growth rates. These parameters were used as supporting evidence rather than as fixed classification thresholds, because particle number concentrations can also be affected by background aerosol levels and local primary emissions.

Based on this re-evaluation, some days originally classified as Undefined, including 12 and 18 April 2025, were reassigned to the unified NPF-day category because their PNSDs and supporting particle-growth characteristics provided sufficient evidence of particle formation and subsequent growth. The remaining Undefined days exhibited enhanced small-particle concentrations or partial modal evolution, but the formation and growth patterns remained too weak, discontinuous, or ambiguous to be classified confidently as NPF. Undefined days were therefore retained as a separate category and included in the non-NPF group only when comparisons between NPF and non-NPF conditions were required.

To improve the transparency and reproducibility of the classification, we have added a day-by-day summary in Table S1. The table provides the revised classification, original growth subgroup, NPF start and end times, mean N_{3-25} and N_{25-100} concentrations, candidate GR time windows, and corresponding GR values for each observation day. Daily PNSD plots for NPF, Undefined, and Non-Event days are presented separately in Figs. S1–S3. Following this revision, the 58 observation days were classified as 43 NPF days, 6 Undefined days, and 9 Non-Event days.

Comment 3:

Monsoon NPF mechanism and NPF mechanism in general:

The study says that monsoon NPF is mainly associated with SO_2 availability and therefore H_2SO_4 formation. This is can also be reasonable, but since the authors couldn't measure all the parameters such as sulfuric acid, or bases such as ammonia or amines, or organic molecules and their oxidation products. SO2 is clearly quite high and therefore can be a reason for the NPF. One possibility could be to calculate Sulphuric Acid proxy from SO2 and see how it compare to the formation rate. Because of all of that I would say that the interpretation that monsoon NPF is sulfur-precursor-driven should be softened unless additional analysis such as at least Sulphuric Acid proxy Vs Formation rate. Also, the paper discusses possible VOC-related oxidation in the pre-monsoon season but cannot constrain it. We understand that these measurements are very complicated, especially in such location, however, considering recent literature on HOMs/OOMs in mountain and TP environments, the author should be more critical in highlighting these limitations. They have a beautiful data set also without going too much in details on the NPF mechanism.

Response 3：

We thank the referee for this important and constructive comment. We agree that the original manuscript placed excessive emphasis on a sulfur-precursor-driven mechanism, considering that gaseous H_2SO_4, ammonia, amines, VOCs, and their oxidation products were not directly measured.

First, because the October – November and March – April campaigns were relatively short and cannot fully represent the broader monsoon and pre-monsoon seasons, we have replaced "monsoon" and "pre-monsoon" with "autumn observation period" and "spring observation period," respectively, throughout the manuscript. We have also avoided generalizing the differences observed during these two campaigns as representative seasonal patterns or mechanisms.

Following the referee's suggestion, we calculated a relative H_2SO_4-related photochemical proxy for periods with concurrent SO_2, $J(O(^1D))$, and CS measurements during the autumn observation period. The proxy was expressed as $[SO_2]\ J(O(^1D))/CS$, representing the potential photochemical production of H_2SO_4 relative to its condensational loss. The calculation method, data-processing procedure, assumptions, and limitations have been added to Sect. S1 of the Supplement. The corresponding results are presented in Fig. S5.

The relative H_2SO_4-related proxy was generally higher on NPF days than on non-NPF days during the particle-formation period, providing additional evidence for an association between sulfur-containing precursor availability and autumn NPF. However, because the spectral measurements required to derive $J(O(^1D))$ were available only during part of the autumn campaign, the proxy analysis did not provide continuous coverage of all observation days. In addition, no site-specific relationship between $J(O(^1D))$, OH, and measured gaseous H_2SO_4 was available. We therefore use the proxy only as a relative indicator and do not interpret it as an absolute H_2SO_4 concentration or as definitive evidence of a uniquely sulfur-driven mechanism.

Accordingly, we have softened the mechanistic interpretation throughout the Abstract, Results and Discussion, and Conclusions. The revised manuscript now states that the higher SO_2 concentrations and enhanced relative H_2SO_4-related proxy on NPF days suggest that sulfur-containing precursors likely contributed to particle formation and early growth during the autumn observation period, rather than demonstrating that sulfur precursors exclusively controlled NPF.

We have also revised the discussion of the spring observation period. The possible contribution of VOC-related oxidation is now presented only as a hypothesis that cannot be constrained by the available measurements. We further emphasize that the absence of direct measurements of H_2SO_4, ammonia, amines, VOCs, HOMs/OOMs, and their oxidation products prevents quantitative attribution of the molecular mechanisms during either observation period. Relevant recent studies of organic compounds and HOMs/OOMs in high-altitude Himalayan and TP environments have been incorporated to provide broader context. These limitations are now explicitly acknowledged in both the mechanism discussion and the Conclusions.

Comment 4:

Urban primary emissions vs NPF:

I think it would be good if the authors could try to better separate regional NPF from local primary ultrafine particle emissions. This could include analysis of wind direction, BC/NO_2/SO_2 spikes, rush-hour timing, and whether events occur simultaneously across broader size ranges. Considering the unique location this would add strength and very interesting new information to the study.

Response 4：

We thank the referee for this important suggestion. We agree that distinguishing atmospheric NPF from local primary ultrafine-particle emissions is particularly important at the urban Tibet University (TU) site. We have therefore strengthened this aspect of the analysis using the available PNSD, size-segregated particle number concentrations, gaseous pollutants, wind conditions, and $PM_{2.5}$ and PM_{10} measurements.

First, the revised NPF classification does not rely solely on an increase in small-particle number concentration. An NPF day requires the appearance of a distinct new particle mode at small diameters followed by identifiable modal growth toward larger sizes. Short-lived particle-number spikes without subsequent systematic growth were not classified as NPF. This criterion helps distinguish atmospheric NPF from primary-emission plumes, which generally produce transient enhancements over relatively fixed size ranges rather than a coherent banana-shaped growth pattern.

Second, the size-segregated diurnal profiles provide additional evidence for this interpretation. On NPF days, the morning increase in N_{3-25} was followed by an enhancement in N_{25-100}, consistent with particle formation and subsequent growth. In contrast, evening enhancements in N_{25-100}, particularly when they occurred without a preceding increase in nucleation-mode particles, may have been influenced by local urban emissions and are now interpreted cautiously in the revised manuscript. Variations in $N_{100-700}$ were comparatively weaker during the principal particle-formation period, indicating that the NPF classification was not based on a simultaneous concentration increase across the entire measured size range.

Third, we compared SO_2, NO_2, and O_3 under different wind directions on NPF and non-NPF days (Figs. 8 and 9). The results showed differences in gaseous pollutants and transport conditions between day types, but no single wind sector or short-lived pollutant enhancement consistently explained all identified NPF events. The aerosol inlet was located approximately 20 m above ground level, which reduced, but did not eliminate, the direct influence of nearby traffic exhaust and resuspended road dust.

Because BC measurements were unavailable, we additionally examined the diurnal variations in $PM_{2.5}$ and PM_{10} for the revised day categories during both observation periods (Fig. R1). The increases in nucleation-mode particle number concentration on NPF days were not accompanied by corresponding daytime spikes in $PM_{2.5}$ or PM_{10} during the principal particle-formation period. Daytime $PM_{2.5}$ concentrations were not higher on NPF days than on Non-Event days, whereas PM_{10} concentrations were broadly comparable between the two categories. These results suggest that the identified events were not simply manifestations of broader fine-particle pollution or dust episodes.

Nevertheless, $PM_{2.5}$ and PM_{10} are mass-based measurements dominated by larger particles and cannot substitute for BC as tracers of traffic-related ultrafine-particle emissions. Moreover, measurements were available at only one site. We therefore cannot fully separate regional-scale NPF from all local primary ultrafine-particle influences or determine the spatial extent of individual events. We have explicitly acknowledged this limitation and have avoided describing the identified events as definitively regional. Instead, the revised manuscript interprets them as atmospheric NPF events observed at an urban site, while recognizing that local urban emissions may affect precursor availability, particle sinks, and parts of the measured ultrafine-particle population. The additional $PM_{2.5}$ and PM_{10} comparison is provided here as Fig. R2 for the referee's evaluation but is not included in the Supplement because these measurements provide supporting evidence rather than direct source tracers.

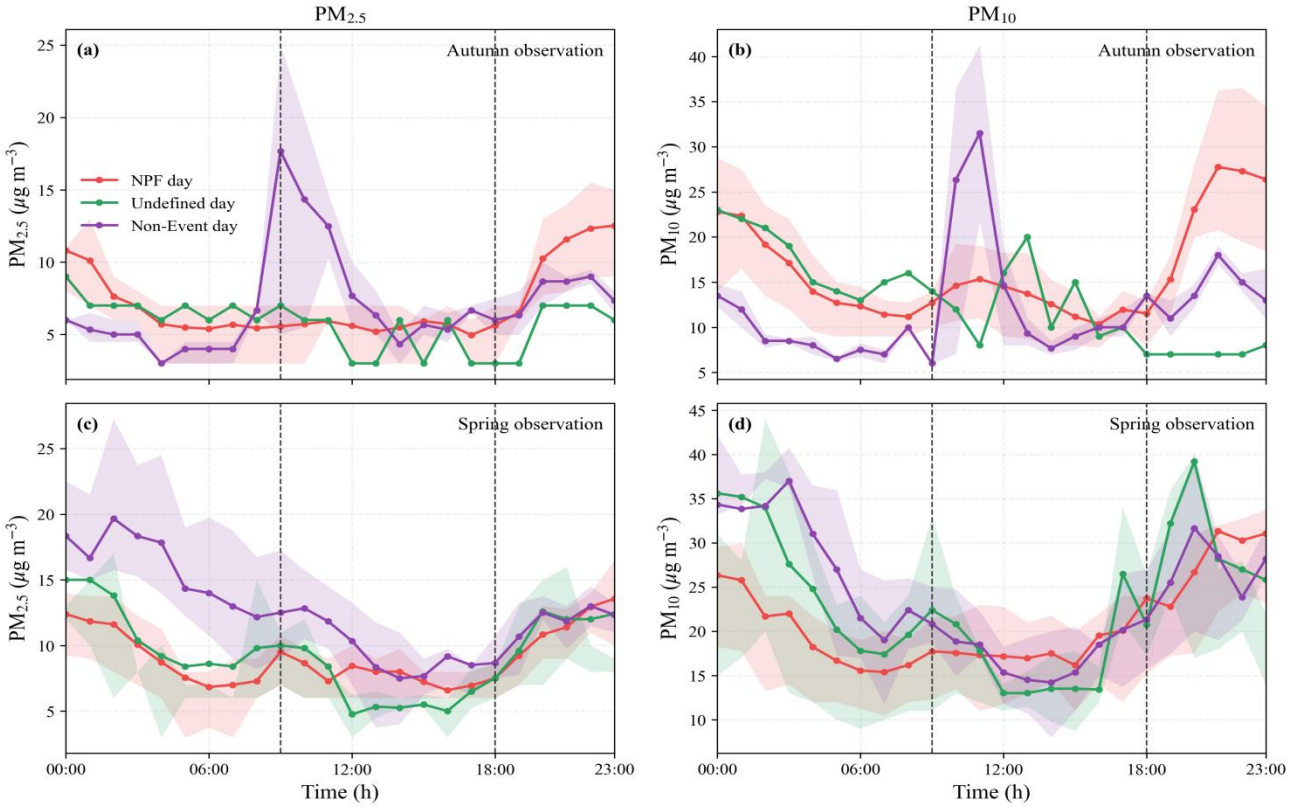

Figure R1. Diurnal variations in $PM_{2.5}$ and PM_{10} concentrations for NPF, Undefined, and Non-Event days during the autumn and spring observation periods. Solid lines represent hourly mean concentrations, and the shaded areas indicate the interquartile ranges. The vertical dashed lines indicate 09:00 and 18:00 local time. $PM_{2.5}$ and PM_{10} are used as supporting indicators of broader particulate-matter pollution and dust influences rather than as direct tracers of traffic-related ultrafine-particle emissions.

Ccomment 5:

Line 25 – Define TU. I guess you mean TP.

Response 5:

Thank you for pointing this out. TU refers to Tibet University rather than the Tibetan Plateau. We have now defined the abbreviation at its first occurrence as "Tibet University (TU)." The abbreviation TP is used separately for the Tibetan Plateau.

Ccomment 6:

Figure 1 – "Tibetan Plateau" is not visible. Also, define TU in the caption.

Response 6:

Thank you for this helpful comment. We have redrawn Fig. 1 using the provincial-level administrative boundaries of China to provide a clearer and unambiguous geographical context for the observation site. The revised figure clearly shows the location of the Tibet Autonomous Region and the Tibet University (TU) observation site. Because the provincial administrative

boundaries do not correspond to the physical geographical extent of the Tibetan Plateau, we have not attempted to delineate or highlight the plateau in the revised map. TU is now explicitly defined as Tibet University in the figure caption.

Ccomment 6:

Figure 2 – Fix the Panel a Y-axes description. Caption is missing explanation.

Response 6:

Thank you for pointing this out. We have corrected the y-axis label in Fig. 2a to particle diameter, Dp (nm), and clarified the color-bar label as $\mathrm{d}N/\mathrm{d}\log D_p$ (cm^{-3}). We have also expanded the caption to explain the content of each panel, the PNSD color scale, the modal fitting curves, and the modal contributions.

Ccomment 6:

Figure 3 – fixe axes labels here as well. Too many overlaps.

Response 6:

Thank you for this suggestion. We have revised the layout of Fig. 3 by adjusting the axis-label positions, font sizes, panel spacing, and legend placement. Overlapping labels and tick marks have been removed, and the axis labels.

Ccomment 6:

Caption in general could contain more information related to the figures.

Response 6:

Thank you for this helpful suggestion. We have reviewed and expanded the captions throughout the manuscript. The revised captions now describe the content of individual panels, define the principal symbols and abbreviations, specify the relevant units and statistical quantities, and explain the meanings of lines, colors, markers, and shaded areas where applicable. This allows the figures to be interpreted more independently from the main text.

Sect. S1 Calculation of the H_2SO_4-related photochemical proxy

Because gaseous H_2SO_4 was not directly measured, a relative H_2SO_4-related photochemical proxy was calculated to examine the possible association between sulfur-containing precursor availability and new particle formation (NPF) during the autumn observation period. The proxy was based on the approximate balance between the photochemical production of H_2SO_4 through OH-initiated oxidation of SO_2 and its condensational loss to the pre-existing aerosol population (Petäjä et al., 2009; Dada et al., 2020):

$$P(H_2SO_4) = [SO_2]\, J(O(^1D))/CS \quad \text{(s1)}$$

where $[SO_2]$ is the molecular number concentration of SO_2, $J(O(^1D))$ is the O_3 photolysis frequency, and CS is the condensation sink. $J(O(^1D))$ was used as an indicator of daytime photochemical OH production because tropospheric OH concentrations are often closely related to solar ultraviolet radiation and O_3 photolysis (Rohrer and Berresheim, 2006). The proxy therefore represents the potential photochemical production of H_2SO_4 relative to its condensational loss.

The SO_2 mixing ratio was converted from ppb to molecular number concentration according to

$$[SO_2] = \chi(SO_2) \times 10^{-9} \times P/(k_B T) \times 10^{-6} \quad \text{(s2)}$$

where $\chi(SO_2)$ is the SO_2 mixing ratio in ppb, P is atmospheric pressure in Pa, T is air temperature in K, and k_β is the Boltzmann constant. A representative pressure of 650 hPa was used for the TU site, and the factor 10^{-6} converts molecules m^{-3} to molecules cm^{-3}.

SO_2, temperature, $J(O(^1D))$, and CS were synchronized and averaged to a common 30 min time resolution. Negative SO_2 values was excluded. Negative $J(O(^1D))$ values attributable to instrumental noise were set to zero, and periods with non-positive or missing CS were excluded. Missing spectral measurements were not interpolated. The proxy was therefore calculated only when concurrent valid measurements of all required variables were available.

The spectral measurements used to derive $J(O(^1D))$ were available only during part of the autumn observation period. Consequently, the proxy analysis does not provide continuous coverage of the entire autumn campaign and was not used to compare the autumn and spring observation periods. Undefined and Non-Event days were combined as non-NPF days for this supplementary comparison.

No site-specific empirical coefficient relating $J(O(^1D))$ to OH or relating the proxy to measured H_2SO_4 was available. Therefore, $P(H_2SO_4)$ was used only as a relative photochemical proxy and should not be interpreted as an absolute gas-phase H_2SO_4 concentration. The proxy also neglects other potential H_2SO_4 sources, such as stabilized Criegee intermediate chemistry, and losses associated with molecular clustering. These omitted pathways may be important, particularly in urban environments (Dada et al., 2020).

Table S1. Day-by-day revised classification, NPF timing, particle number characteristics, and candidate particle growth rates during the two observation periods. Mean $N_{3–25}$ and $N_{25–100}$ concentrations were calculated over 09:00–18:00 local time. Candidate $GR_{3–7}$ and $GR_{7–20}$ values were evaluated for every observation day by linear regression of automatically identified continuous modal trajectories. No R^2 threshold was applied. "NA" indicates that insufficient data or no sufficiently long and continuous trajectory was available.

Date	Revised classification	Original growth subgroup	NPF window	Mean $N_{3–25}$ (# cm^{-3})	Mean $N_{25–100}$ (# cm^{-3})	$GR_{3–7}$ window	$GR_{3–7}$ (nm h^{-1})	$GR_{7–20}$ window	$GR_{7–20}$ (nm h^{-1})
Oct 9, 2024	NPF day	Class II	8:40–14:30	16954	4977	08:42–09:12	4.26	09:17–14:27	1.62
Oct 10, 2024	NPF day	Class II	9:00–15:00	10803	4047	NA	NA	09:22–14:57	1.94
Oct 16, 2024	NPF day	Class I	9:00–21:00	19292	8532	09:02–09:32	3.90	09:37–17:57	0.93
Oct 17, 2024	NPF day	Class II	9:00–14:00	16605	5433	NA	NA	09:07–13:57	2.19
Oct 18, 2024	NPF day	Class II	8:40–14:30	16091	5005	08:42–09:27	3.47	09:32–14:27	1.35
Oct 19, 2024	NPF day	Class II	9:00–15:00	6346	3912	09:02–09:37	1.80	09:42–14:57	2.35
Oct 20, 2024	NPF day	Class II	9:00–18:00	21295	6244	09:02–13:07	0.17	09:42–17:52	1.30
Oct 22, 2024	NPF day	Class I	9:00–22:00	20350	6818	09:02–16:37	-0.02	09:37–17:57	-0.42
Oct 23, 2024	NPF day	Class II	9:00–15:00	12206	4174	NA	NA	09:02–14:57	0.93
Oct 24, 2024	NPF day	Class I	9:00–23:00	11971	4732	09:02–09:32	5.30	09:37–17:57	0.53
Oct 25, 2024	NPF day	Class I	9:00–21:00	11913	4686	09:02–09:47	3.60	09:52–17:57	1.21
Oct 26, 2024	NPF day	Class I	9:30–23:00	12083	3157	09:32–13:52	0.08	10:07–17:57	1.06
Oct 27, 2024	NPF day	Class I	9:30–22:00	15552	6391	NA	NA	09:47–17:57	1.28
Oct 28, 2024	NPF day	Class I	9:00–24:00	16668	5924	NA	NA	09:22–17:57	1.10
Oct 29, 2024	NPF day	Class I	9:30–24:00	10131	5355	NA	NA	09:47–17:57	1.43
Oct 30, 2024	NPF day	Class I	9:30–24:00	8331	4331	NA	NA	09:52–17:57	1.12
Oct 31, 2024	NPF day	Class I	9:30–21:00	9420	6128	NA	NA	10:02–17:57	0.78

Date	Revised classification	Original growth subgroup	NPF window	Mean $N_{3–25}$ (# cm^{-3})	Mean $N_{25–100}$ (# cm^{-3})	$GR_{3–7}$ window	$GR_{3–7}$ (nm h^{-1})	$GR_{7–20}$ window	$GR_{7–20}$ (nm h^{-1})
Nov 1, 2024	NPF day	Class I	9:30–24:00	18403	6892	NA	NA	10:02–17:57	0.85
Nov 2, 2024	NPF day	Class I	9:00–24:00	19211	7233	09:02–09:32	5.17	09:37–17:57	1.16
Nov 3, 2024	NPF day	Class I	9:00–21:00	14440	6669	09:02–09:52	3.13	09:57–17:57	1.31
Nov 4, 2024	NPF day	Class II	12:00–16:00	4937	3492	NA	NA	12:02–15:57	3.34
Nov 7, 2024	NPF day	Class I	9:00–24:00	24496	8216	NA	NA	09:27–17:57	0.49
Nov 8, 2024	NPF day	Class I	9:30–24:00	16717	8280	NA	NA	09:52–17:57	0.72
Nov 9, 2024	NPF day	Class I	9:30–24:00	14049	6956	NA	NA	09:42–17:57	1.08
Nov 10, 2024	NPF day	Class I	9:30–24:00	10546	5078	NA	NA	10:02–17:57	1.34
Mar 25, 2025	NPF day	Class I	9:00–21:00	13321	3237	NA	NA	09:25–18:00	1.05
Mar 26, 2025	NPF day	Class I	9:00–21:00	8415	3265	09:00–09:35	3.36	09:40–18:00	1.17
Mar 27, 2025	NPF day	Class II	9:00–17:00	15776	3581	NA	NA	09:20–17:00	0.60
Mar 28, 2025	NPF day	Class II	9:00–14:00	12317	2713	NA	NA	09:20–13:40	2.22
Mar 30, 2025	NPF day	Class II	9:00–11:00	3715	561	09:00–09:35	4.33	09:40–10:55	4.73
Apr 2, 2025	NPF day	Class II	8:30–12:30	7511	1182	08:30–09:35	1.67	09:40–12:30	1.49
Apr 6, 2025	NPF day	Class II	8:30–13:00	13406	1586	NA	NA	08:30–12:55	0.98
Apr 7, 2025	NPF day	Class II	8:30–12:30	8616	2079	08:30–09:00	5.78	09:05–12:25	2.16
Apr 8, 2025	NPF day	Class II	8:30–16:30	9734	1750	08:30–09:10	3.92	09:15–16:25	0.95
Apr 9, 2025	NPF day	Class II	9:00–16:00	6494	3110	09:00–09:35	3.48	09:40–15:55	1.60
Apr 12, 2025	NPF day	Undefined	9:00–11:00	4131	2176	NA	NA	09:20–10:55	8.44
Apr 13, 2025	NPF day	Class II	9:00–16:00	9928	2010	09:00–09:40	3.51	09:45–15:55	1.22
Apr 16, 2025	NPF day	Class II	8:30–16:00	11387	5571	NA	NA	09:00–15:55	1.28
Apr 17, 2025	NPF day	Class I	8:00–18:00	16775	6852	NA	NA	08:30–17:55	1.03

Date	Revised classification	Original growth subgroup	NPF window	Mean $N_{3–25}$ (# cm^{-3})	Mean $N_{25–100}$ (# cm^{-3})	$GR_{3–7}$ window	$GR_{3–7}$ (nm h^{-1})	$GR_{7–20}$ window	$GR_{7–20}$ (nm h^{-1})
Apr 18, 2025	NPF day	Undefined	11:00–14:00	5239	1392	NA	NA	11:25–13:55	1.59
Apr 19, 2025	NPF day	Class II	8:30–18:00	10978	3950	NA	NA	08:50–17:55	1.15
Apr 21, 2025	NPF day	Class I	8:00–21:00	15983	4139	08:00–08:30	2.95	08:35–17:55	0.93
Apr 22, 2025	NPF day	Class II	9:00–16:00	9488	1375	NA	NA	09:15–15:55	0.46
Oct 15, 2024	Undefined	Undefined	NA	2042	1142	07:17–12:57	-0.14	07:02–17:57	0.44
Mar 29, 2025	Undefined	Undefined	NA	2946	644	13:35–14:25	0.67	07:00–17:55	-0.28
Apr 10, 2025	Undefined	Undefined	NA	3888	819	NA	NA	07:00–17:55	-0.05
Apr 11, 2025	Undefined	Undefined	NA	5214	989	NA	NA	07:00–17:45	-0.02
Apr 14, 2025	Undefined	Undefined	NA	2597	1219	NA	NA	07:05–17:55	0.60
Apr 20, 2025	Undefined	Undefined	NA	4855	873	NA	NA	07:20–17:55	0.40
Oct 21, 2024	Non-Event	Non-Event	NA	2011	1117	12:32–13:42	-0.72	07:02–17:57	0.39
Nov 5, 2024	Non-Event	Non-Event	NA	1034	2292	07:12–17:57	-0.25	07:02–17:17	0.80
Nov 6, 2024	Non-Event	Non-Event	NA	1085	2751	NA	NA	07:02–17:57	-0.35
Mar 31, 2025	Non-Event	Non-Event	NA	517	366	14:35–17:00	0.07	07:00–17:15	-0.88
Apr 1, 2025	Non-Event	Non-Event	NA	170	410	13:50–14:25	0.52	14:30–18:00	0.49
Apr 3, 2025	Non-Event	Non-Event	NA	688	401	07:35–10:55	-0.19	07:00–18:00	-0.15
Apr 4, 2025	Non-Event	Non-Event	NA	245	443	NA	NA	07:20–18:00	-0.01
Apr 5, 2025	Non-Event	Non-Event	NA	254	585	NA	NA	07:00–17:55	0.16
Apr 15, 2025	Non-Event	Non-Event	NA	846	1023	NA	NA	07:00–17:35	-0.37

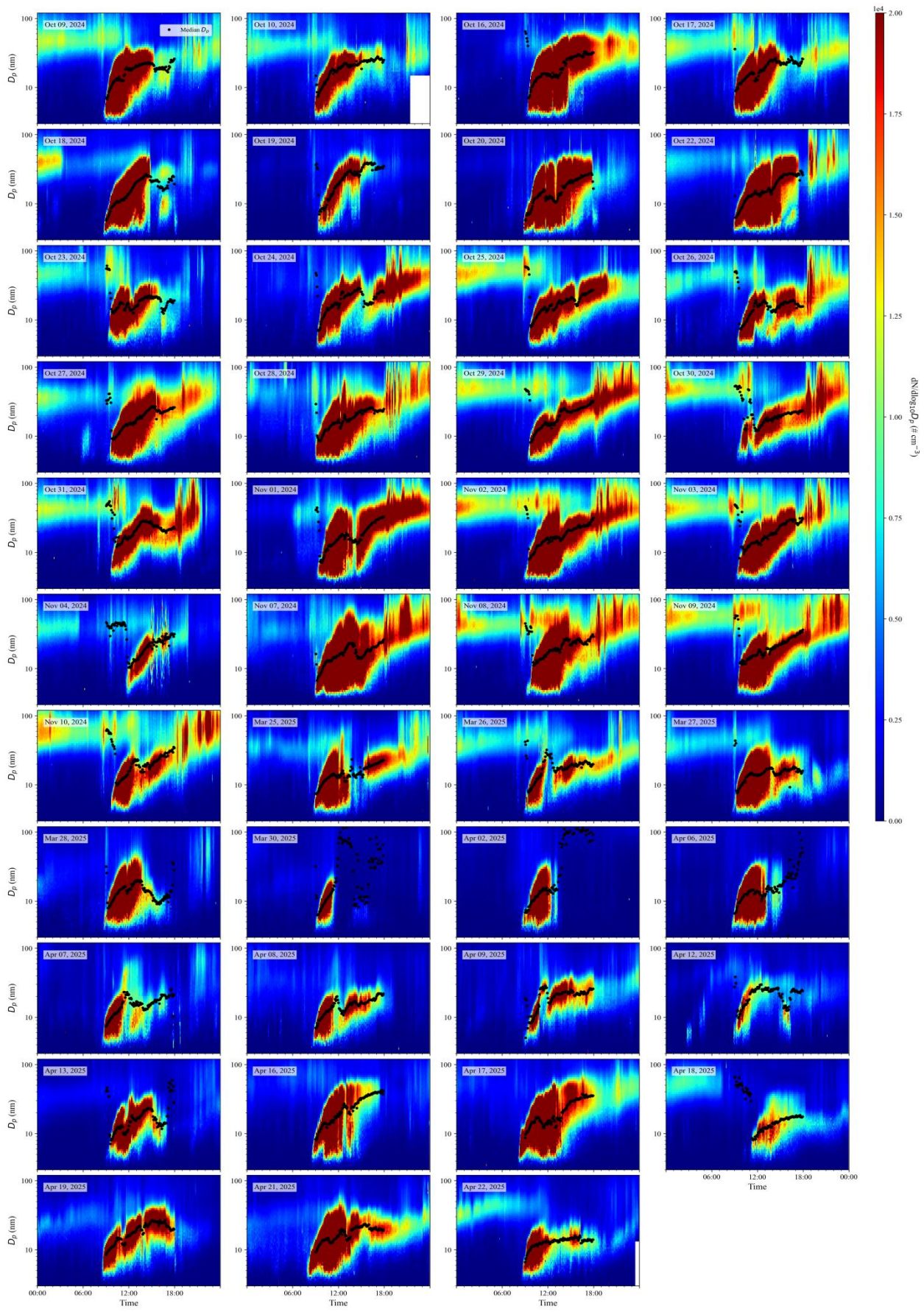

Figure S1: PNSDs for all NPF days. Each panel represents one day. The black dots indicate the median particle diameter.

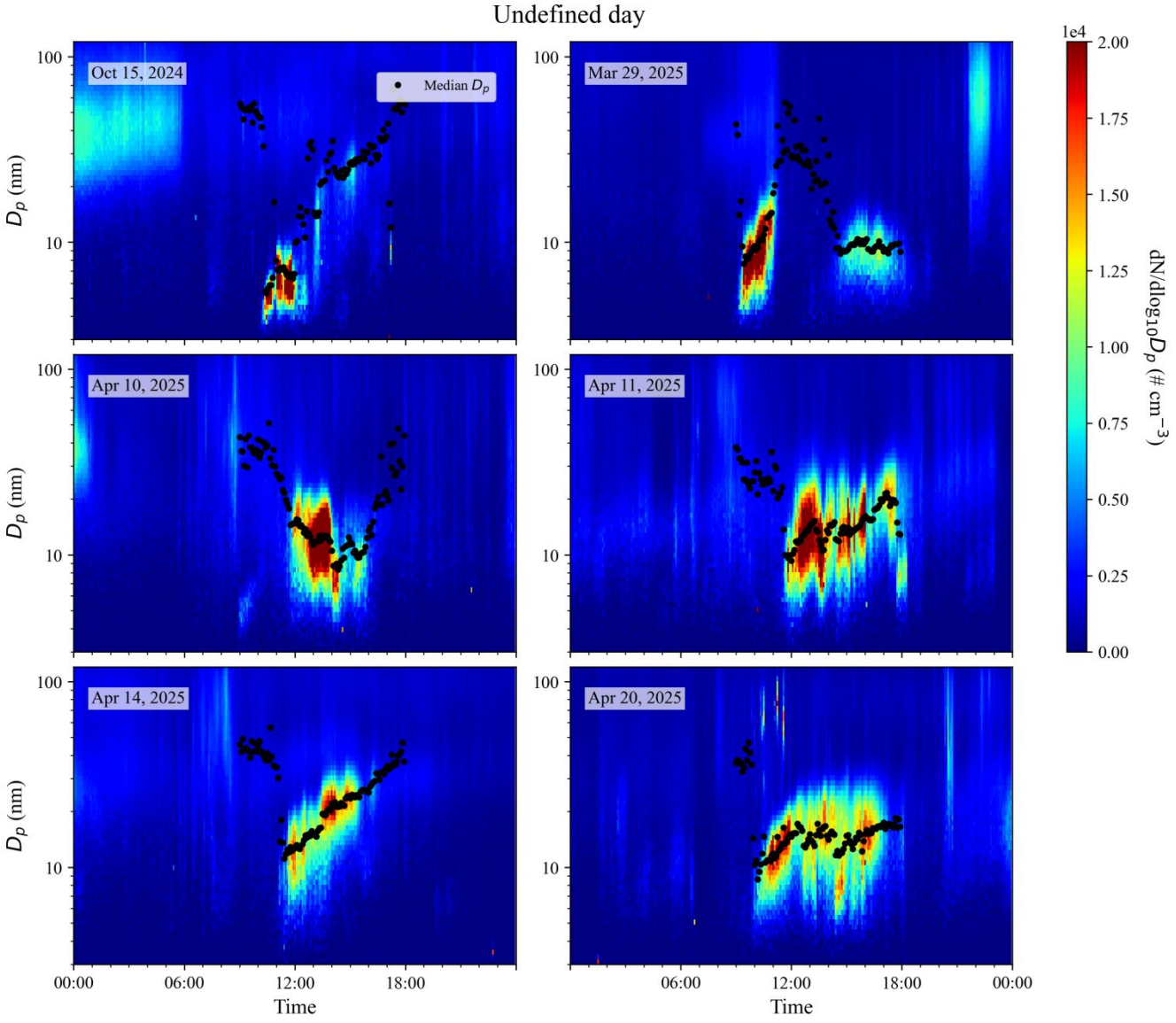

Figure S2: PNSDs for all Undefined days. Each panel represents one day. The black dots indicate the median particle diameter.

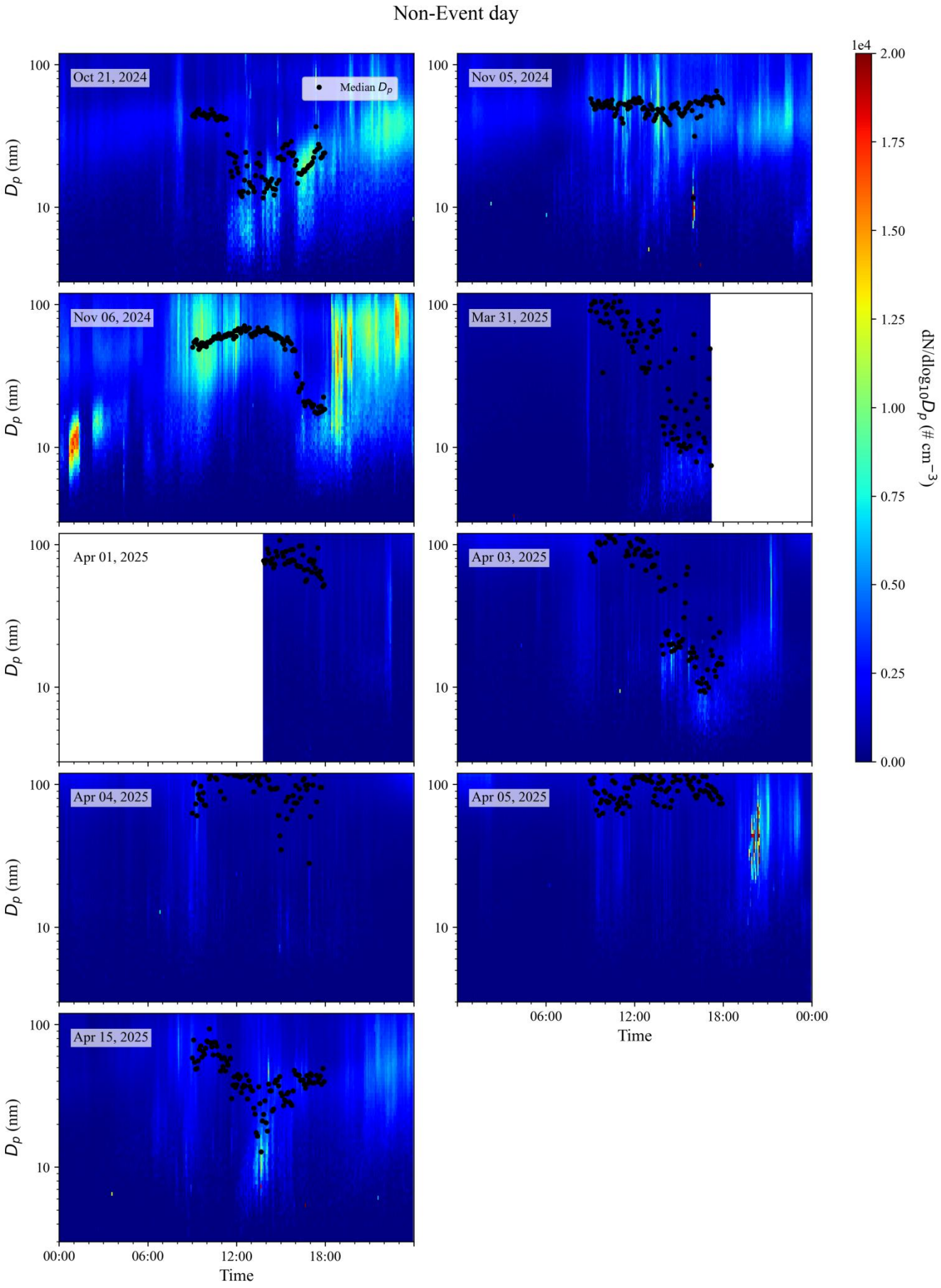

Figure S3: PNSDs for all Non-Event days. Each panel represents one day. The black dots indicate the median particle diameter.

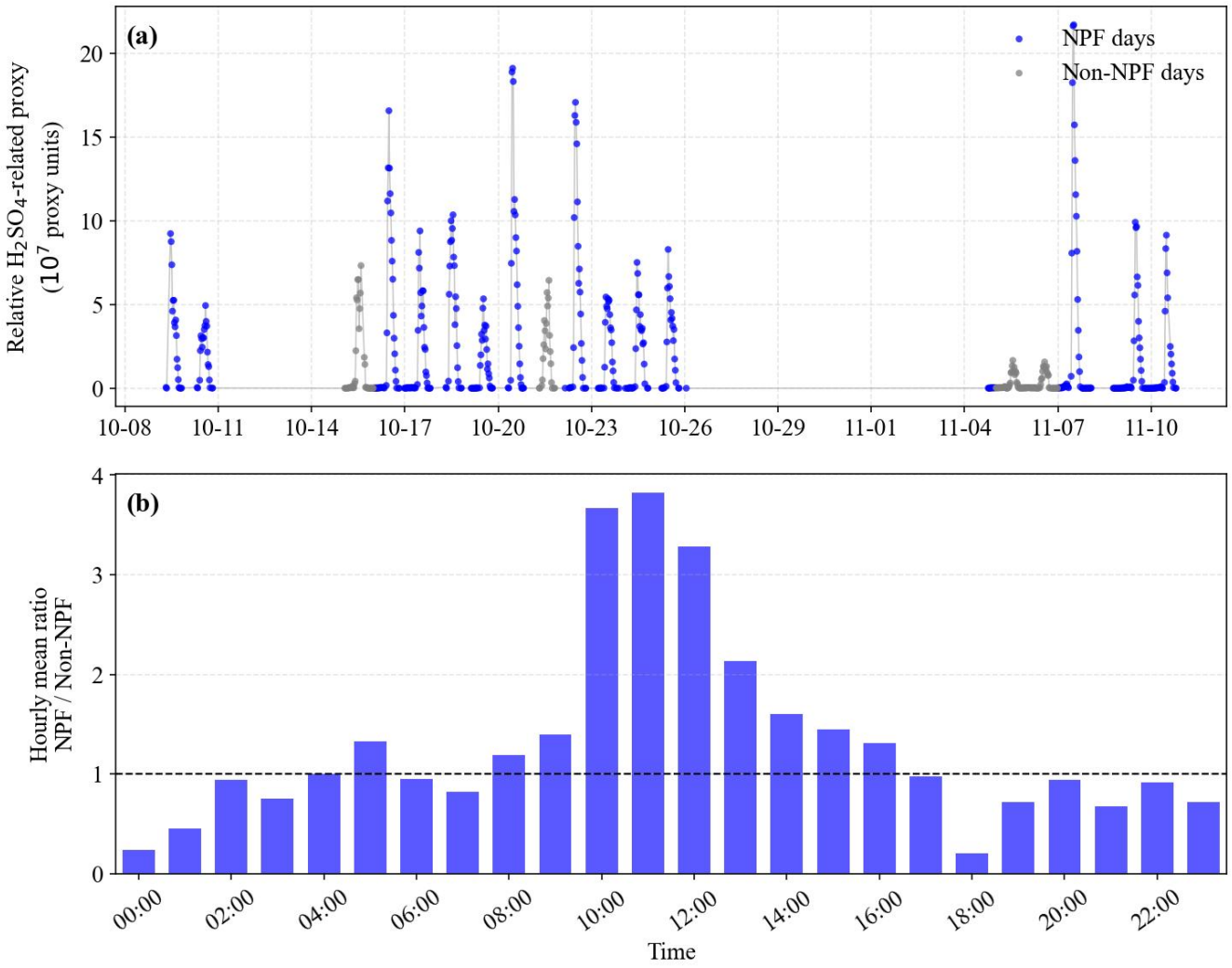

Figure S5: H_2SO_4-related photochemical proxy during periods with available spectral measurements in the autumn observation period. (a) Time series of the 30 min proxy values on NPF and non-NPF days. (b) Ratio of the hourly mean proxy on NPF days to that on non-NPF days.

References

Dada, L., Ylivinkka, I., Baalbaki, R., Li, C., Guo, Y., Yan, C., Yao, L., Sarnela, N., Jokinen, T., Daellenbach, K. R., Yin, R., Deng, C., Chu, B., Nieminen, T., Wang, Y., Lin, Z., Thakur, R. C., Kontkanen, J., Stolzenburg, D., Sipilä, M., Hussein, T., Paasonen, P., Bianchi, F., Salma, I., Weidinger, T., Pikridas, M., Sciare, J., Jiang, J., Liu, Y., Petäjä, T., Kerminen, V. M., and Kulmala, M.: Sources and sinks driving sulfuric acid concentrations in contrasting environments: implications on proxy calculations, Atmos. Chem. Phys., 20, 11747–11766, 10.5194/acp-20-11747-2020, 2020.

Petäjä, T., Mauldin, I. R. L., Kosciuch, E., McGrath, J., Nieminen, T., Paasonen, P., Boy, M., Adamov, A., Kotiaho, T., and Kulmala, M.: Sulfuric acid and OH concentrations in a boreal forest site, Atmos. Chem. Phys., 9, 7435–7448, 10.5194/acp-9-7435-2009, 2009.

Rohrer, F. and Berresheim, H.: Strong correlation between levels of tropospheric hydroxyl radicals and solar ultraviolet radiation, Nature, 442, 184–187, 10.1038/nature04924, 2006.